Effect of the precipitates on the hydrogen desorption kinetics from zirconium-niobium alloys

C. Juillet, M. Tupin, F. Martin, Q. Auzoux, C. Berthinier, F. Gaudier, T. Guilbert, C. Toffolon

Effect of the precipitates on the hydrogen desorption kinetics from zirconium-niobium alloys

C. Juillet[(1)], M. Tupin[(2)], F. Martin[(1)], Q. Auzoux[(1)], C. Berthinier[(3)], F. Gaudier[(4)], T. Guilbert[(5)], C. Toffolon[(5)]

(1) Université Paris-Saclay, CEA, Service de la Corrosion et du Comportement des Matériaux dans leur Environnement, 91191, Gif-sur-Yvette, France

(2) Université Paris-Saclay, CEA, Service d'Etude des Matériaux Irradiés, 91191, Gif-sur-Yvette, France

(3) Université Paris-Saclay, CEA, Service d'Etude Mécaniques et Thermiques, 91191, Gif-sur-Yvette, France

(4) Université Paris-Saclay, CEA, Service de Thermohydraulique et de Mécanique des Fluides, 91191, Gif-sur-Yvette, France

(5) Université Paris-Saclay, CEA, Service de Recherches Métallurgiques Appliquées, 91191, Gif-sur-Yvette, France

Keywords: Hydrogen; Desorption kinetics; Precipitates; Thermal desorption mass spectrometry; Zr-Nb alloys

1 Abstract

This study aims at identifying and quantifying the rate-limiting steps of the hydrogen desorption process from unoxidized M5**Framatome** alloy. Gaseous deuterium charging, Thermal Desorption Spectrometry (TDS), Differential Scanning Calorimetry (DSC) and finite elements simulations of TDS results reveal that hydrogen desorption kinetics from the metal is limited by the surface molecular recombination (similarly to Zircaloy-4) and that part of the hydrogen originated from the elaboration process of M5**Framatome** and Zr-2.5%Nb is trapped by the Nb-rich precipitates. In the studied conditions and regarding M5**Framatome**, the desorption flux corresponding to this initially trapped hydrogen reaches its maximum after the total dissolution of the precipitates, which releases hydrogen into solid solution. The kinetic constant corresponding to surface recombination identified on M5**Framatome** was identical to the one previously determined on Zircaloy-4.

2 Introduction

Zirconium-based alloys are widely used as nuclear fuel rod cladding material in pressurized water reactor (PWR) owing to their low capture cross section of thermal neutrons and good mechanical properties. Among them, $M5_{\textbf{Framatome}}$ alloy (Zr-1%Nb) developed and licensed by Framatome (so-called M5 here-after) proved to have a better corrosion resistance and a much lower hydrogen uptake than Zircaloys alloys under normal operating conditions in PWRs [1,2].

The hydrogen contained within the claddings has three possible origins: (i) elaboration process, (ii) corrosion in primary water, both dealing with protium species, and finally (iii) ternary fission products as tritium species. During the elaboration process, a small hydrogen amount is absorbed into the metal leading to an initial hydrogen concentration of around 0.0025 wt.% [3]. Under normal operating conditions in PWRs, the external surface of zirconium alloy fuel cladding is exposed to primary water and continuously oxidized, process during which the cladding absorbs a fraction of the hydrogen atoms produced by water reduction [4,5]. This fraction is itself partitioned between the metal and the oxide layer, in different proportions according to the affinity and transport properties of hydrogen in each solid phase (in terms of solubility and diffusivity). In the fuel rod, ternary fission occurring within the uranium oxide fuel leads to the formation of tritium, part of which can then be absorbed and potentially diffuse through the cladding. During drying, transport, reprocessing or storage of used nuclear fuels, hydrogen and tritium may desorb from the cladding, which implies safety concerns. A closer understanding of hydrogen/tritium transport phenomena is a keystone for a better estimation of hydrogen/tritium potential release.

As already exposed in reference [6], the hydrogen release from the alloy can be decomposed into five elementary steps:

1. Hydrogen diffusion via interstitial sites through the alloy towards the metal/oxide interface [7];
2. Integration into the oxide lattice by crossing the metal/oxide interface;
3. Diffusion through the oxide towards the subsurface;
4. Passing from subsurface sites to surface sites as adsorbed species;
5. Final recombination into dihydrogen molecules and desorption from the oxide surface.

In previous studies [6,8], we studied the hydrogen desorption from a Zircaloy-4 (referred to as Zy4 thereafter) sheet. The only source of hydrogen considered in that case was internal hydrogen coming

from the material elaboration process. We showed that hydrogen desorption kinetics from the unoxidized alloy was limited by its molecular recombination reaction on the surface. By coupling modelling programmed by finite elements (FE) with Cast3M code [9] and URANIE optimization tool [10], we quantified the desorption rate constant k'_{des} with an activation energy and a pre-exponential factor equal to 290 ± 10 kJ mol^{-1} and 3 x 10^7 m^4 mol^{-1} s^{-1} respectively. The use of Zy4 in PWRs is decreasing as more advanced alloys are supplanting it. It is therefore crucial to study also the release process of hydrogen and tritium from more recent cladding materials such as M5 alloy.

Zy4 and M5 have both an α-Zr hexagonal compact structure. The diffusion coefficients of hydrogen in these alloys are very close as for other pure α-structured zirconium alloys [11–20]. The major differences between Zy4 and M5 lay in their global chemical composition and their Secondary Phase Particles (SPPs) nature and distribution. Most alloying elements included in zirconium alloys have indeed a low solubility in α-Zr (hcp) matrix [21]. Alloying elements in Zy4 are mainly tin, iron and chromium , the last two forming inter and intra-granular Laves phases, $Zr(Fe,Cr)_2$ [22,23]. The M5 alloy contains mainly 1 wt.% of niobium instead of tin. Two types of precipitates in this alloy are observed Laves phases $Zr(Nb,Fe)_2$ and β-(Zr,Nb) precipitates, the latter containing about 85 wt.% of niobium [24].

The potential role of such SPPs in hydrogen transport (diffusion and trapping) in the alloy may be questioned. Following Density Functional theory simulations by Burr *et al.* [25,26], the intermetallic precipitates $ZrFe_2$ and $ZrCr_2$ are not able to trap hydrogen whereas, niobium-containing precipitates such as $ZrNb_2$ would. Calculated solution enthalpy for an interstitial hydrogen atom in β-Nb was similar to that in α-Zr. The niobium-rich precipitates could thus modify the hydrogen distribution, transport or desorption kinetics. The main investigation technique used to monitor hydrogen desorption is Thermal Desorption Spectrometry (TDS) [6,8,27,28], for which a temperature ramp is applied to the specimen, typically between 293 and 1273 K. In this temperature range, many phase transformations may occur (starting with the α/β phase transformation) that could interfere with hydrogen desorption and affect the signal analysis.

Differential Scanning Calorimetry (DSC) studies were carried out by Toffolon [29,30] in order to investigate the phase transformation kinetics of SPPs for both alloys. The heating rate was 5 K min^{-1} and revealed that the SPPs dissolution occurred at lower temperature for the zirconium-niobium alloys (about 923 – 973 K for M5 alloy [29] and between 873 K and 1033 K for quaternary alloys Zr-Nb-Sn-Fe [30]) than for Zy4 alloy (around 1073 K [30]). Using also DSC experiments, Forgeron *et al.* [31] showed that the allotropic transformation from α-Zr (hcp) to β-Zr (bcc) phase happened at higher temperature (1023 K and 1083 K for M5 and Zy4, respectively) at the thermodynamic equilibrium.

This study is aimed at identifying the rate limiting step of the hydrogen desorption kinetics from unoxidized M5 specimens, quantifying the desorption rate constant and studying the SPPs influence on the hydrogen desorption. To reach these goals, the TDS technique was extensively used to measure hydrogen desorption kinetics. It was associated with High Sensitivity Differential Scanning Calorimetry measures (HS-DSC). HS-DSC study enabled to determine the various microstructural evolutions during a temperature ramp typical of a TDS analysis. Finite elements using the Cast3M code [6,9] coupled with URANIE optimization tool [10] were used to analyze these data and extract the most probable values for the different kinetic constants involved in the hydrogen desorption rate-limiting step. Ultimately, the desorption processes between M5 and Zy4 are compared and discussed. In order to investigate the potential difference in the desorption process of the hydrogen originated from the elaboration process and the hydrogen absorbed after the elaboration, two different kinds of specimens were used: uncharged samples and deuterium charged samples. Please note that the results and discussion regarding the deuterium charged specimens are presented only in section 4.6. The other following sections refer to uncharged specimens containing hydrogen that originated from the elaboration process exclusively.

3 Experimental Procedure

3.1 Material and specimen preparation

0.45 mm-thick sheets of recrystallized M5 and Zr-2.5Nb alloys were used. They were supplied by Framatome and ATI™, respectively. The chemical composition of the alloys used in this study is given in Table 1. For the M5 alloy, the hydrogen concentration was measured by the inert-gas melting extraction technique (using thermal conductivity in a Galileo G8, Bruker GmbH) on a set of 10 specimens. The average initial concentration was about 104 ± 20 mol m^{-3}. Before TDS experiments, the specimens (1 cm^2) were ground with SiC paper and submitted to a final polishing with ¼ µm diamond paste. The final sample thickness was around 0.35 mm. Specimens were rinsed in deionized water then cleaned in acetone-ethanol solution and dried in air.

Table 1. Chemical composition of the M5 and Zr-2.5%Nb alloys used in the present study.

Alloying elements	Nb wt.%	O wtppm	Fe wtppm	H wtppm	Zr
M5	1	1400	400	13 – 19	Bal.
Zr-2.5%Nb	2.5	1100	1200	10	Bal.

3.2 Thermal Desorption Spectrometry

The desorption kinetics of hydrogen was measured by Thermal Desorption Spectrometry (TDS). TDS set-up used in this study, developed at CEA, is made of a quartz tube under vacuum (10^{-6} – 10^{-7} mbar) wherein the specimen is inserted, surrounded by a cylindrical furnace and coupled to a quadrupole mass spectrometer (Transpector 100-M INFICON^{TM}). By imposing a temperature ramp up to 1273 K, the specimen is heated up. Desorbed species are then ionized, separated, detected and counted by the mass spectrometer. Hydrogen species are quantified thanks to the H_2 calibration previously realized. The hydrogen amount desorbed from the specimen during the TDS experiment was estimated by integrating the calibrated signal as a function of time during the experiment.

3.3 High sensitivity calorimetry

Calorimetry experiments were carried out using a Setaram Multi HTC high-temperature high-sensitivity calorimeter in order to follow the phase transition during the heating. This technique measures a heat flow between a sample and an inert reference during a thermal cycle. Experiments were conducted under inert gas (pure argon or helium) at a heating rate of 10 K min^{-1}. Microstructural changes such as the allotropic phases transformations (α→β), and the phenomena of secondary phases precipitation/dissolution (intermetallic, β-Nb precipitates) undergone by the sample during this cycle were deduced from the obtained data.

3.4 Gaseous deuterium charging

For gaseous deuterium charging, each specimen was inserted in a quartz tube (200 mL). A heat treatment at 873 K during 1 h under vacuum (10^{-4} mbar) was first carried out in order to dissolve the native oxide layer. Deuterium gas was then injected into the tube at room temperature in amounts corresponding to – once absorbed – 50 wtppm equivalent hydrogen in the alloy (*i.e.* 100 wtppm of deuterium). Deuterium charging lasted 1 h at 873 K. During subsequent cooling, deuterium precipitates as zirconium hydrides (deuterides) [16,32–34]. According to Kearns' investigations on hydride dissolution in Zy4 [35], for such a hydrogen concentration, the formed hydrides will dissolve quickly and at relatively low temperature (below 573 K) during the TDS temperature ramp.

4 Results and discussion

4.1 Thermal desorption spectrometry experiments

Figure 1 compares the hydrogen desorption flux obtained on M5 specimens and Zy4 samples [6,8] for two temperature ramp rates, 10 K min^{-1} and 7 K min^{-1}, respectively. The temperature for TDS experiments varies in the range from 293 K to 1273 K.

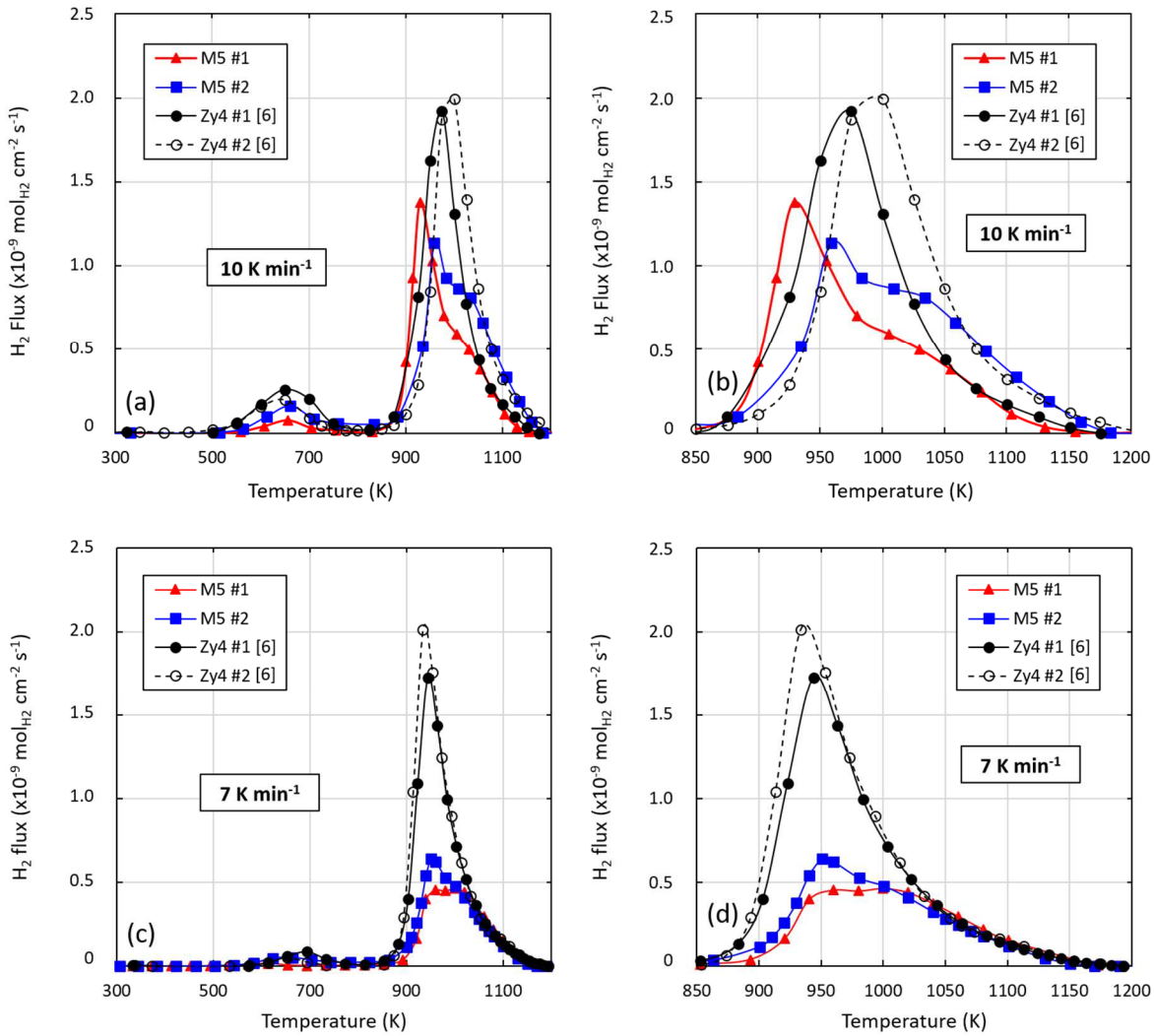

Fig. 1. Comparison of the H_2 fluxes measured by TDS during a temperature ramp at: (a – b) 10 K min^{-1} and (c – d) 7 K min^{-1} on two as-prepared M5 samples (red triangles and blue squares) and Zy4 alloy *[6]* (full and empty black circles).

TDS curves corresponding to the experiments on M5 samples (red triangles and blue squares curves) show three hydrogen desorption peaks (one little peak around 650 K and a main peak around 950 K

with a shoulder at higher temperature). Thermograms corresponding to Zy4 samples (black circles) only present two peaks (one little peak around 650 K and a main peak around 950 K without any shoulder). This likely suggests that the first two peaks (650 K and 950 K) would result from the same two desorption mechanisms for both M5 and Zy4.

Hydrogen released at around 650 K (first TDS peak) is a product of the residual water reduction present in the quartz device [6]. A rough estimation of the oxide layer thickness formed during the temperature ramp up to 773 K was obtained by integrating the first hydrogen desorption peak and neglecting the hydrogen absorption [6]: around 10 ± 5 nanometers. At room temperature, a native oxide layer (a few nanometers) forms on the surface of zirconium alloys owing to the high affinity of zirconium for oxygen and its low redox potential [11,36,37]. This thin oxide layer may block or reduce hydrogen release from the alloy, by acting as a diffusion barrier [38]. During TDS experiments, at temperatures around 750 K the specimens are consequently covered by an oxide layer of approximately 20 nm (native oxide plus oxide formed during experiment), which eventually turns out to dissolve into the alloy when temperature rises [6]. This oxide layer dissolution during the TDS temperature ramp was evaluated by simulation of oxygen diffusion in the M5 alloy and is presented in section 4.2.

For Zy4 alloy, the second desorption peak was assigned to the desorption of the hydrogen contained in the alloy (solid solution hydrogen), the rate limiting step of this desorption being the surface recombination reaction [6]. This peak was shifted towards higher temperatures in the presence of an oxide layer [8]. For M5 alloy, this peak was accompanied by another one: a shoulder at slightly higher temperature. As mentioned earlier, the first high temperature peak may correspond to the desorption of hydrogen in interstitial sites positions as for Zy4 alloy, but the second one has to be assigned to desorption from other sites, generally referred to as traps. As pointed out in the introduction, the main difference between M5 and Zy4 alloys lies in their precipitates. SPPs may indeed impact the hydrogen desorption kinetics in different ways, acting either as traps for hydrogen, or as “hot/cold spots” for hydrogen surface recombination, for instance. Keeping abovementioned assumptions concerning the desorption peak around 950 K, an hypothesis concerning the peak at higher temperature for M5 alloy (around 1050 K) would be that it corresponds to the desorption of the hydrogen initially trapped in deep trapping sites (*i.e.* needing high thermal activation to untrapp). The niobium-containing precipitates encountered in M5 alloy are highly probable candidates for such traps, since no equivalent signal was observed during desorption from Zy4 alloy. Study of these high temperature peaks constitute the main body of the following sections.

4.2 Simulation of the oxygen dissolution

The objective here is to estimate the temperature corresponding to the complete dissolution of the 20 nm-thick oxide layer and to compare it with the temperature corresponding to the onset of hydrogen desorption from the alloy (high temperature peaks) in order to determine the surface state (metallic or oxide) of the sample when hydrogen desorbs.

Following the methodology described in our previous works [6,8], *i.e.* solving numerically by finite elements the diffusion process of oxygen in the M5 alloy matrix, taken into consideration the actual TDS temperature ramp as input data, the 20 nm-thick oxide layer was found to be completely dissolved at 833 K. This result is based on the assumption of an uniform dissolution process (see discussion in [6,8]).

For M5 alloy, the two high temperature hydrogen desorption peaks appear above 900 K, after this theoretical total oxide layer dissolution. They are therefore both representative of hydrogen desorbing from the metal, without any oxide layer on the surface, which simplifies the studied system.

4.3 Modelling of the hydrogen desorption including a contribution from the hydrogen trapped by SPPs

Since hydrogen desorption occurs after the full theoretical oxide layer dissolution, the system can be considered as purely metallic and steps (2) (integration into the oxide lattice) and (3) (diffusion process through the oxide) described in the introduction are not relevant anymore. Therefore, the hydrogen that is already in interstitial solid solution follows steps (1) (diffusion process through the metal), (4) (transition from subsurface to surface) and (5) (recombination into molecules and desorption). According to our assumption, the hydrogen that is trapped in Nb-rich precipitates need first to detrapp from these sites into interstitial sites before following the same steps, *i.e.* the diffusion process through the metal up to desorption. The sketch in Figure 2 illustrates the new system in M5 alloy during TDS, for temperatures above 833 K.

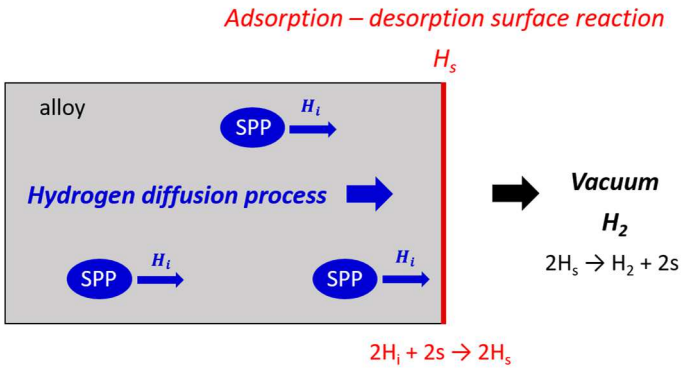

Fig. 2. Sketch of the system considered for hydrogen desorption from the alloy at temperatures above 833 K, including release of hydrogen from Nb-rich precipitates into the matrix.

Based on the results obtained by Wilde on titanium [39] and our previous study on Zy4 [6], step (4) (transition from subsurface to surface) was assumed to be much faster than step (5) (recombination into molecules and desorption). Step (4) is thus considered to be at equilibrium. In this case, the hydrogen surface coverage is assumed to be proportional to the interstitial hydrogen concentration at the vicinity of the surface (subsurface). The system is hereby reduced to three possible rate-limiting steps, *i.e.* detrapping, diffusion or recombination.

The hydrogen desorption model presented in [6], which includes diffusion and surface recombination, was updated in order to take into account hydrogen detrapping from niobium-containing precipitates. Please note that this model is intended to represent hydrogen desorption kinetics but is not relevant for hydrogen absorption and particularly trapping phenomena.

Under these hypothesis, the diffusion equation must be solved with terms for sources and sinks for traps, as done by McNabb and Foster considering the chemical reaction (Eq.1) and associated coupled equations (Eq.2) and (Eq.3) for modified diffusion (modified Fick's second law) and trapping/detrapping [40]. McNabb and Foster's set of equations is commonly used in steels [41] and nickel [42,43].

$$\mathrm{H} + [\ ]_{\mathrm{trap}} \underset{\mathrm{k_p}}{\overset{k_l}{\rightleftarrows}} [\mathrm{H}]_{\mathrm{trap}} \qquad \text{(Eq.1)}$$

In Eq.1, H represents a single hydrogen atom in an interstitial site, $[\ ]_{\mathrm{trap}}$ a free trap site, and $[\mathrm{H}]_{\mathrm{trap}}$ a trapped hydrogen atom, with k_p and k_l the respective trapping and detrapping kinetic constants. This reaction deems one H atom per trap site maximum and assumes that traps are not interconnected (dilute system hypothesis), meaning that hydrogen in traps have to be released in the

matrix before interacting further. Here only one type of trap site is assumed, and hypothesis is made that the trap sites are initially fully occupied, meaning that the trap site occupancy fraction at initial time θ(t=0) equals 1.

$$\frac{\partial C_{H_i}}{\partial t} + N\frac{\partial \theta}{\partial t} = \vec{\nabla} \cdot \left(D_{H_i} \overrightarrow{\nabla(C_{H_i})} \right) \quad \text{(Eq.2)}$$

$$\frac{\partial \theta}{\partial t} = k_p(1-\theta)C_{H_i} - k_l\theta \quad \text{(Eq.3)}$$

In Eq.2 and Eq.3, C_{H_i} is the local interstitial hydrogen concentration (mol m^{-3}), θ the trap site occupancy fraction, N the trap site density (mol_{trap} m^{-3}), D_{H_i} the hydrogen diffusion coefficient in the alloy equal to $(3.2 \pm 2.5).10^{-7} \exp\left(-\frac{38000 \pm 5000}{RT}\right)$ m^2 s^{-1} [11–20], k_p and k_l the hydrogen trapping and detrapping kinetic constants, respectively in m^3 s^{-1} mol^{-1} and s^{-1}. Note that in the calculations performed in the present work, N is kept constant whatever the temperature, meaning that all possible modifications such as defects annealing or else during the temperature ramp are neglected.

It is assumed that each kinetic constant, k_p and k_l, follows an Arrhenius relationship, involving an activation energy (E_p and E_l, expressed in J mol^{-1}) and a pre-exponential constant (k_p^0 and k_l^0).

The hydrogen recombination and desorption process at the surface is described by the following reaction (Eq.4):

$$2H_i \xrightarrow{k'_{des}} H_2 + 2V_i \quad \text{(Eq.4)}$$

with H_i an interstitial hydrogen atom in subsurface, V_i a free interstitial site in the hcp lattice, and H_2 a dihydrogen molecule released in vacuum.

The hydrogen recombination and desorption rate at the surface is given by the following expression (Eq.5):

$$\varphi_{H_2} = k'_{des}\left(C_{H_i}\right)^2 \qquad (mol_{H2}\ m^{-2}\ s^{-1}) \quad \text{(Eq.5)}$$

where k'_{des} is the desorption rate constant (m^4 mol_{H2}^{-1} s^{-1}).

However, the hydrogen desorption rate computed in Cast3M code is not exactly equation (Eq.5). It is indeed expressed, for numerical commodity, as follows (Eq.6):

$$\varphi_{H_2} = \frac{k_{des}}{2C_{Hi}^{init}}\left(C_{H_i}\right)^2 \qquad (mol_{H2}\ m^{-2}\ s^{-1}) \quad \text{(Eq.6)}$$

with C_{Hi}^{init} the initial interstitial hydrogen concentration in the metal (mol m^{-3}) and k_{des} a desorption rate constant expressed in m s^{-1} and linked to the k'_{des} rate constant according to the following formula (Eq.7):

$$k_{des} = 2 \times C_{Hi}^{init} \times k'_{des} \quad \text{(Eq.7)}$$

The initial interstitial hydrogen concentration in the metal C_{Hi}^{init} is also equal to the difference between the total initial hydrogen concentration in the metal C_H^{tot} (mol m^{-3}) and the initial hydrogen concentration in the traps N (mol m^{-3}).

The desorption rate constant depends on the temperature according to the following Arrhenius law (Eq.8):

$$k_{des} = k_{des}^0 . \exp\left(-\frac{Ea_{des}}{RT}\right) \quad \text{(Eq.8)}$$

with Ea_{des} the activation energy for desorption (J mol^{-1}) and k_{des}^0 a pre-exponential factor (m s^{-1}). As seen previously (section 4.1), the desorption peak from hydrogen in solid solution starts at the same temperature for both M5 and Zy4. The same value of the pre-exponential factor k'^0_{des} determined for Zy4 (k'^0_{des}= 3.10^7 m^4 mol^{-1} s^{-1}) [6] was therefore used for M5. Nevertheless, a potential difference between the values of the activation energy of the surface recombination rate Ea_{des} of M5 and Zy4 was taken into account. Beyond determining the value of Ea_{des} for M5, our goal is to quantify the kinetic parameters E_l, k_l^0 and the trap site density *N* associated with the second high temperature peak for M5 alloy. Based on TDS experimental data, a numerical optimization plan for the quantification of these parameters was undertaken with help of the URANIE software [6,10]. The kinetic parameters corresponding to the trapping were not included in the optimisation plan of this study mainly dedicated to detrapping and desorption. Following section is dedicated to the description of this work.

4.4 Determination of the kinetic constants by FE methods based on TDS experimental data

The desorption peaks positions and relative intensities obtained during TDS experiments depend on the temperature ramp rate. Such dependence on the temperature ramp have been widely used in TDS thermograms analysis [44–47], and provide a sufficiently large thermogram landscape to be used as reference data for code testing, quantification and optimization. For the present study, TDS

experiments were carried out on M5 samples at different heating rates, varying between 1 and 10 K min^{-1} (two samples were tested at 7 K min^{-1} to check reproducibility). Figure 3 shows the influence of the ramp rate on the hydrogen desorption flux. The third desorption peak seems to disappear for the slowest ramp rate but is actually present in the form of the long tail at high temperatures. Desorption data corresponding to the two samples tested at 7 K min^{-1} are relatively similar, excepted for the intensity of the first high temperature peak. In all thermograms presented here, the second peak is broader than the first one, suggesting a correspondence to a process with a lower activation energy.

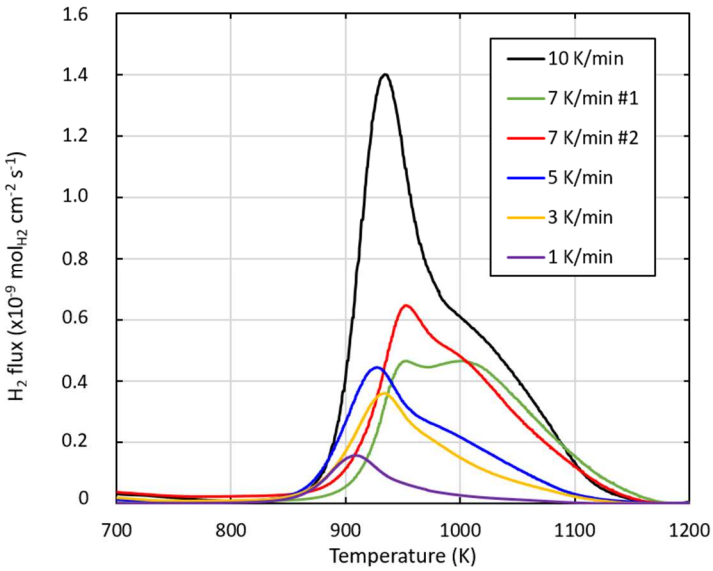

Fig. 3. TDS spectra obtained on M5 samples for signals corresponding to mass 2 (H_2) during a temperature ramp of: 10 K min^{-1} (black curve), 7 K min^{-1} (green and red curves), 5 K min^{-1} (blue curve), 3 K min^{-1} (yellow curve) and 1 K min^{-1} (purple curve). For full colour quality figure, the reader is invited to consult the online version of the paper.

These six TDS experiments were used to identify the optimized value of parameters Ea_{des}, E_l, k_l^0 and *N*. The Cast3M-URANIE coupling procedure is detailed in our previous paper [6]. The URANIE sample tool generates a dot matrix with random quadruplet values with the LHS (Latin Hypercube Sampling) methodology. For each quadruplet of values and each temperature ramp (1 K min^{-1}, 3 K min^{-1}, 5 K min^{-1}, 7 K min^{-1} and 10 K min^{-1}), the FE code (Cast3M) simulates the associated hydrogen TDS thermogram. Then the normalized squared difference between the calculated data and the experimental ones is calculated by Cast3M using the following formula (Eq.9):

$$RR_i = \frac{\sum_j (F_{simu}(x_j) - F_{exp}(x_j))^2}{\max\left(\sum_k (F_{simu}(x_k))^2,\ \sum_l \left(F_{exp}(x_l)\right)^2\right)} \quad \text{(Eq.9)}$$

where RR_i is called a partial error criterion for experiment "i", $F_{simu}(x_j)$ and $F_{exp}(x_l)$ are the simulated flux at the abscissa x_j and the experimental one at abscissa x_l, respectively (temperature on the x-axis). Subscript "i" (i ∈ {1;2;3;4;5;6}) refers to following experiments: {1} for the one at 10 K min^{-1}, {2} for the first one at 7 K min^{-1}, {3} for the second one at 7 K min^{-1}, {4} for the one at 5 K min^{-1}, {5} for the one at 3 K min^{-1} and {6} for the one at 1 K min^{-1} TDS.

Manual simulations were first carried out to restrict the investigated domain for each parameter to be optimized. The ranges of investigation were thereafter set as indicated in Table 2.

Table 2. Parameters used in the numerical resolution with their ranges of investigation.

θ	D_{H_i} (m^2 s^{-1})	k_p (m^3 mol^{-1} s^{-1})	$\ln(k_l^0)$	E_l (kJ mol^{-1})	N (mol m^{-3})	Ea_{des} (kJ mol^{-1})
At t = 0 θ = 1	$10^{-7}\exp\left(-\frac{35000}{RT}\right)$	$0.06\exp\left(-\frac{35000}{RT}\right)$	18 – 30	225 – 305	1 – 30	278 – 294

URANIE sampling tool was then used to determine the minimum of the error criterion for each experiment. Table 3 presents the quadruplet values $\{Ea_{des},\ E_l,\ \ln(k_l^0),\ N\}$ corresponding to the minimum error criterion for each experiment.

Table 3. Optimized values of the kinetic constants parameters and the total hydrogen concentration obtained for the six tested temperature ramp rates.

	10 K min^{-1} (RR1)	7 K min^{-1} #1 (RR2)	7 K min^{-1} #2 (RR3)	5 K min^{-1} (RR4)	3 K min^{-1} (RR5)	1 K min^{-1} (RR6)	Average and range
C_H^{tot} (mol m^{-3})	103	76	85	75	92	95	88 ± 15
$\ln(k_l^0)$	23.1	23.7	20.8	23.7	26.6	24.5	24 ± 3
E_l (kJ mol^{-1})	246	240	229	252	280	274	254 ± 27
N (mol m^{-3})	18.9	20.2	22.5	16.0	15.4	8.8	17 ± 8
Ea_{des} (kJ mol^{-1})	282	291	291	280	289	290	287 ± 7

For each TDS experiment, the amount of hydrogen desorbed from the specimen after reaching 850 K was quantified by integrating the hydrogen desorption flux as a function of time and converted into hydrogen homogeneous concentration C_H^{tot} according to specimen geometry.

The final optimized detrapping kinetic constant (k_l) and the activation energy of desorption (Ea_{des}) are equal to $2.6\text{x}10^{10} \exp\left(-\frac{254 \pm 27 \text{ kJ mol}^{-1}}{\text{RT}}\right)$ s^{-1} and 287 ± 7 kJ mol^{-1}, respectively. As expected, the Ea_{des} value for M5 alloy is identical to the one obtained on Zy4 alloy (290 ± 10 kJ mol^{-1}) [6].

The values of the kinetic constant parameters indicated in Table 3 were used to simulate the six TDS experiments with the FE code. For all the investigated ramp rates, Figure 4 compares the experimental TDS desorption data (black continuous line) with the simulated ones (red dotted line). This figure shows that the upgraded model used, taking into account the hydrogen detrapping process, representing hydrogen release from the precipitates, is able to simulate the presence of two peaks in the hydrogen desorption from M5 alloy, although with some difficulties in terms of shapes and peak positions. In particular, the poor simulation of the last hydrogen desorption peak by our model, especially the decreasing slope of the second peak, suggests that the trapping/detrapping equation may not be perfectly adapted to the real physical phenomenon representative of the hydrogen desorption from the precipitates.

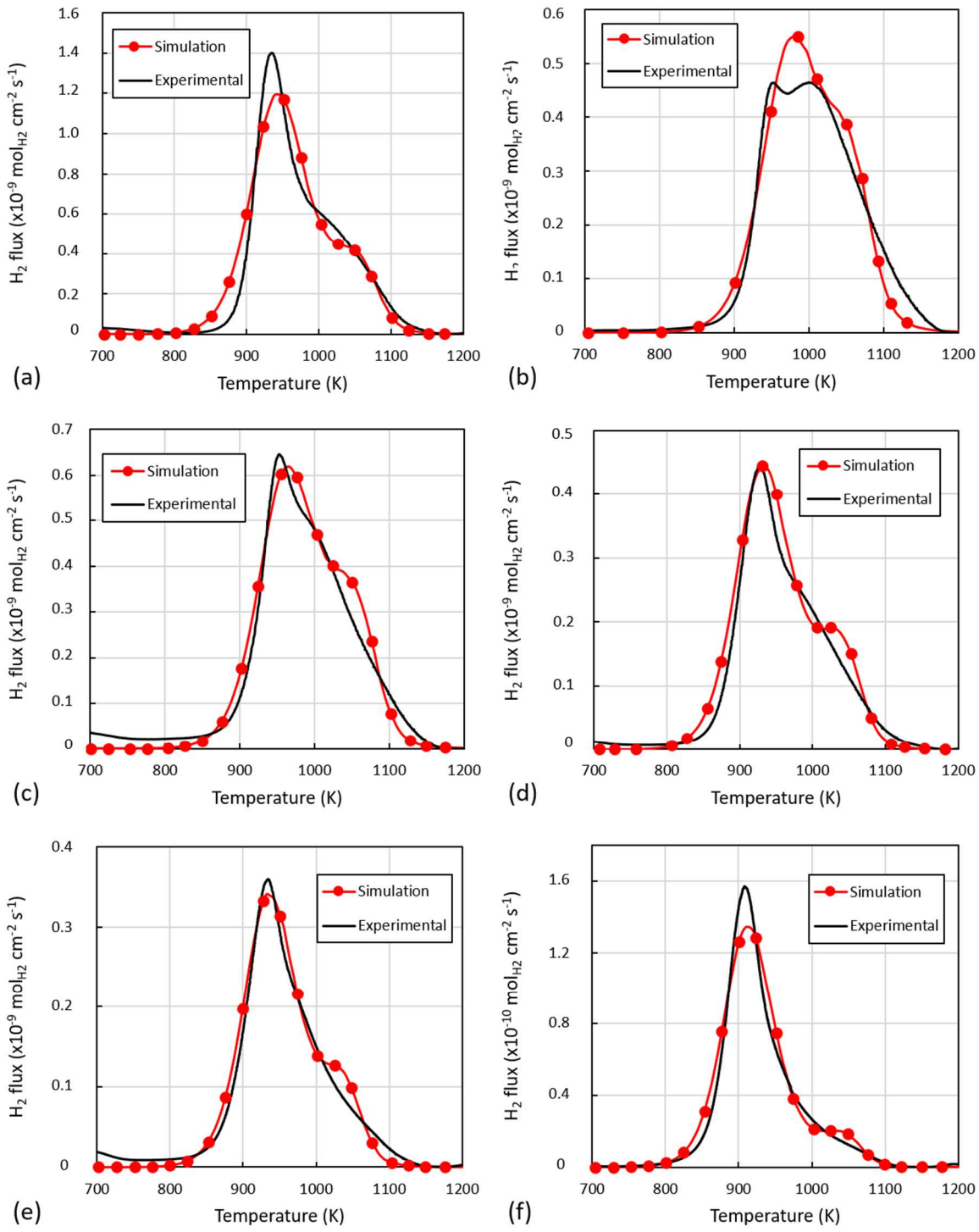

Fig. 4. Comparison between simulated (red dots) and experimental (black line) H_2 desorption flux obtained by FE calculations (Cast3M code) and TDS for different temperature ramps: (a) 10 K min^{-1}; (b) 7 K min^{-1} - first experiment; (c) 7 K min^{-1} - second experiment; (d) 5 K min^{-1}; (e) 3 K min^{-1} and (f) 1 K min^{-1}. Parameters used for each ramp are those given in columns in Table 3.

A plot of the ratio of N to C_H^{tot} obtained by the optimisation process is presented in Figure 5. It indicates that this supposedly constant ratio varies with the temperature ramp rate. This is in

contradiction with the hypothesis stating that the trap density *N* (related to the density of niobium-containing precipitates) is constant throughout the whole temperature ramp.

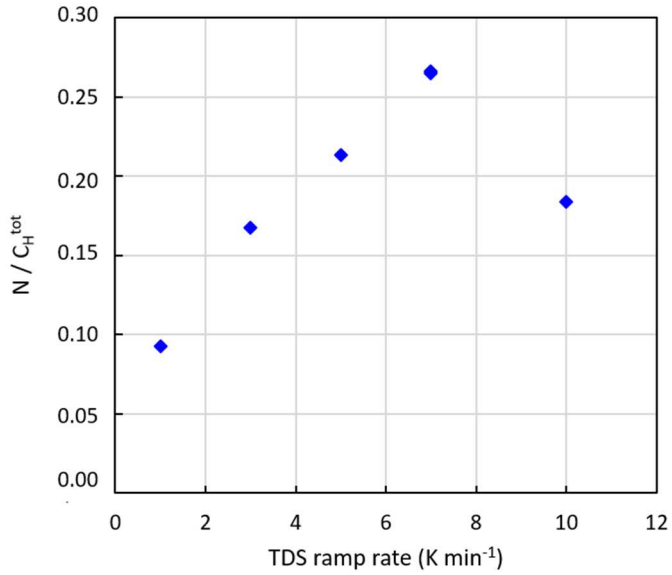

Fig 5. Evolution of the N / C_H^{tot} ratio as function as the temperature ramp rate.

These discrepancies between simulations and experimental results suggest some evolution of the niobium-containing precipitates density during the TDS experiment. According to literature [29–31], at high temperatures, niobium-containing precipitates undergo a phase transformation. During this phase transformation process (or dissolution), a release of hydrogen into the matrix could be expected. Therefore, the dissolution of the precipitates could be one of the hydrogen release rate-limiting steps. The next section is dedicated to investigating the dissolution of these precipitates and the α/β allotropic phase transformation by HS-DSC.

4.5 Phase transformations occurring during TDS temperature ramps

In link with the aforementioned precipitate-dissolution limited hydrogen desorption hypothesis, this section focuses on the phase transformations in M5 alloy during temperature ramps. Figure 6 shows the α/β allotropic phase transformation and compares the transformed fraction from βNb to βZr deduced by calorimetry (HS-DSC) with the TDS desorption flux of hydrogen obtained at identical temperature ramp rates (10 K min^{-1} and 3 K min^{-1}) for both experiments.

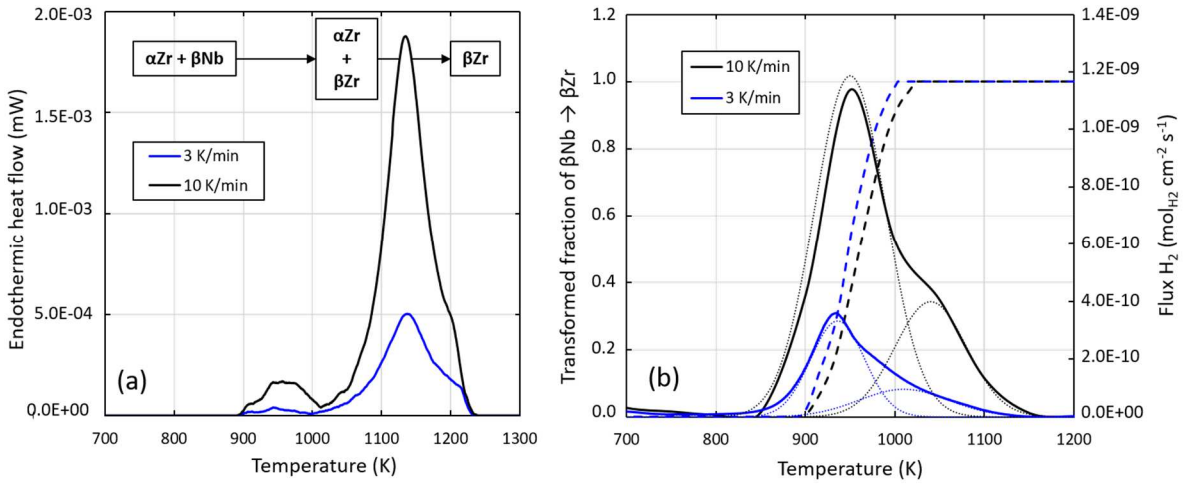

Fig. 6. (a) Endothermic heat flow thermograms obtained by calorimetry on as-received M5 sample submitted to a 10 K min^{-1} (black line) and 3 K min^{-1} (blue line) temperature ramp. (b) Comparison between transformed fraction of βNb → βZr obtained by calorimetry (dashed lines, the left ordinates) and hydrogen desorption flux (continuous lines, right ordinates) on as-received M5 samples submitted to a 10 K min^{-1} (black lines) and 3 K min^{-1} (blue lines) temperature ramp as function of temperature. Gaussian peak deconvolutions into 2 peaks of the TDS data are shown in dotted lines.

Figure 6a reveals the SPPs dissolution occurred between 900 and 1023 K in accordance with Toffolon's observations [29]. The DSC experiments also show that the allotropic transformation from α-Zr (hcp) to β-Zr (bcc) phase begins at 1023 K as indicated by Forgeron's work [31]. In Figure 6b, the deconvolution of the TDS desorption curves into two peaks with a Gaussian shape is presented, in order to separate the contribution from the hydrogen initially in interstitial sites (first peak) and the contribution from the hydrogen initially trapped by the precipitates (second peak). The α/β allotropic phase transformation occurs mainly after the second hydrogen desorption peak indicating that hydrogen desorption is not controlled by the α/β allotropic phase transformation. It appears that the maximum dissolution rate lays in-between the two TDS peaks. In addition, as observed for the hydrogen desorption fluxes, the transformation βNb → βZr is also slightly shifted towards lower temperatures for a slower ramp. Table 4 indicates that the temperature corresponding to the desorption peak related to hydrogen initially trapped by the precipitates and the temperature corresponding to full β-Nb precipitates dissolution are very close for both studied temperature ramp rates.

Table 4. Comparison between the maximum temperature of the third thermodesorption peak and the temperature when the transformed fraction of βNb → βZr equal to one deduced from Figure 6.

	Maximum temperature of the third thermodesorption peak	Temperature at which the transformed fraction of βNb → βZr

		equals 1
10 K min^{-1}	1040 K	1023 K
3 K min^{-1}	1010 K	1003 K

To summarise, during the temperature ramp towards high temperatures, it seems that the hydrogen trapped by Nb-rich precipitates is released in solid solution only when these precipitates dissolve; hydrogen atoms are then free to diffuse in the α-Zr matrix and to desorb from the specimen after surface recombination into molecules. It would therefore be more relevant to implement the hydrogen desorption model with a kinetic law representative of precipitate dissolution, instead of a hydrogen detrapping law with a constant trap density. This implementation and associated simulations will be the subject of further work.

4.6 Desorption of the hydrogen absorbed after the elaboration

The results and discussion presented in the previous sections correspond to the study of uncharged M5 specimens, and address only desorption of the hydrogen that was taken up during the elaboration process. However, under normal operating conditions in PWRs, the global concentration of hydrogenated species increases owing to the hydrogen absorption process occurring during the corrosion of the cladding. The study of a potential hydrogen trapping by the precipitates after the elaboration as well as its impact on the hydrogen desorption kinetics is the subject of the present section.

Gaseous deuterium charging was used, followed by thermal desorption experiments, to trace and differentiate hydrogen species absorption and trapping induced by environmental exposure from hydrogen species issued from the elaboration process.

In addition to M5, a Zr-2.5%Nb alloy, which present higher volumic fraction of niobium-containing precipitates, was studied. These alloys contained initially a metastable phase enriched in niobium. To obtain an α-Zr microstructure, a thermal aging of 5000 h in the α phase temperature domain (at 843 K and 798 K for Zr-2.5%Nb and M5 alloys respectively) was carried out. The obtained microstructures were detailed in Toffolon's thesis [48]. During thermal aging, almost all of the hydrogen initially present in the alloys desorbed: the final hydrogen concentrations, measured by the inert-gas melting extraction technique, were around 4 ± 1 wtppm for both alloys.

As described in section 3.4, gaseous deuterium charging was carried out at 873 K during 1 h on the two alloys in order to reach a deuterium concentration of around 50 wtppm equivalent H (*i.e.* 100

wtppm of D). Figure 7 compares the desorption flux of the different hydrogen species (H_2, HD and D_2) obtained on M5 and Zr-2.5%Nb samples (after thermal aging and gaseous deuterium charging). These TDS experiments were conducted from 293 K up to 1273 K with a 10 K min^{-1} temperature ramp rate.

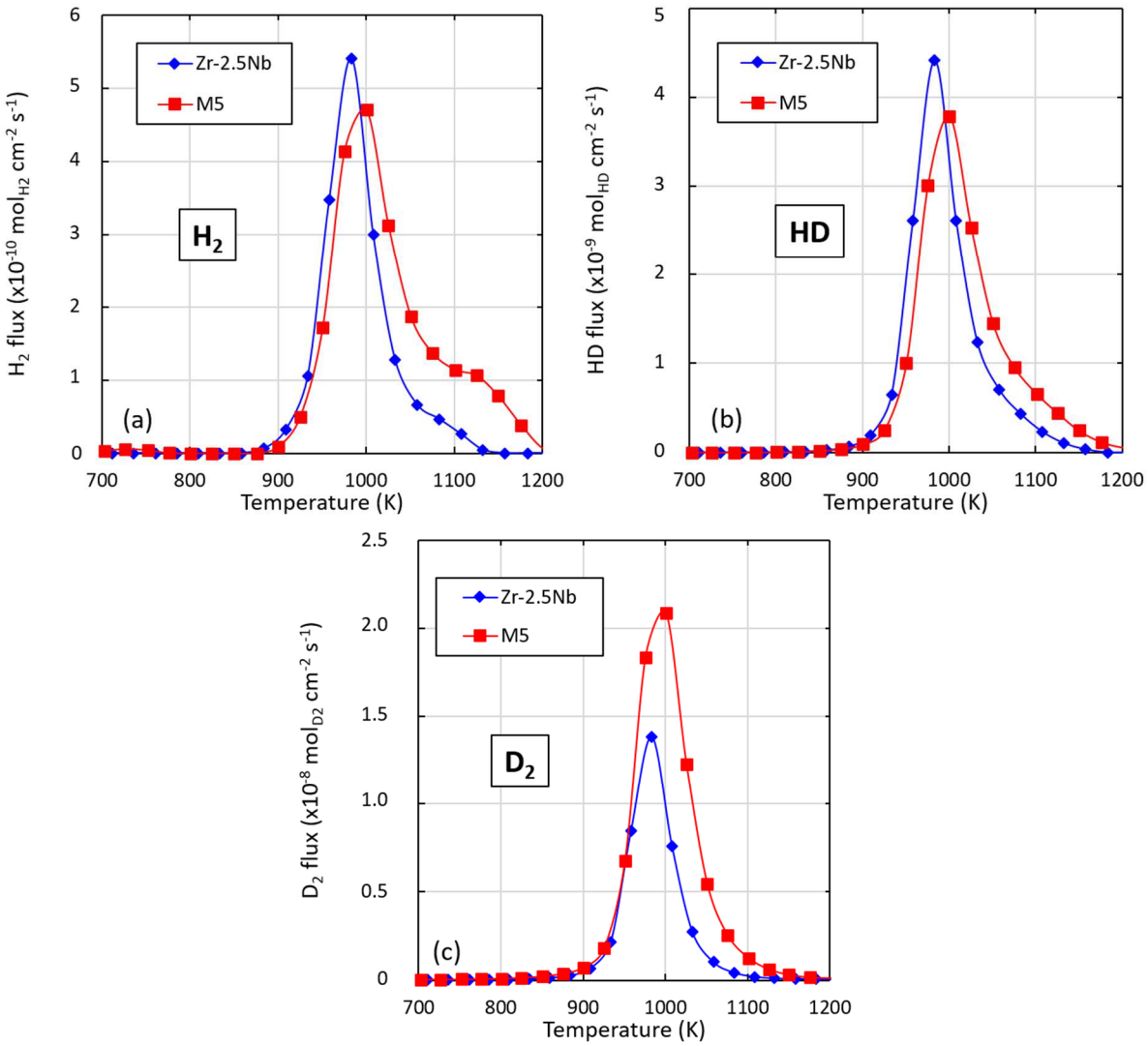

Fig. 7. Hydrogen and deuterium desorption flux comparison between Zr-2.5%Nb (blue diamonds) and M5 (red squares) after thermal aging followed by gaseous deuterium charging: (a) H_2 flux, (b) HD flux and (c) D_2 flux.

As expected, Figure 7 shows that, for both alloys, the main desorption flux corresponds to the D_2 form. The maximum D_2 desorption fluxes take place at the same temperature for M5 and Zr-2.5%Nb, *i.e.* around 1000 K. Unlike deuterium atoms, voluntarily introduced by gaseous charging, the hydrogen (^1H) atoms come from elaboration process. Basically, D_2 signal gives therefore indication on desorption of species introduced as tracer of environmental uptake, whereas H_2 signal provides information on hydrogen introduced in the alloy during its elaboration. HD signal is a mixture of both.

Two hydrogen desorption peaks in H_2 form are observed in Figure 7a, as found earlier: the first hydrogen desorption peak corresponds to the hydrogen in solid solution and the second peak to hydrogen trapped by the precipitates during elaboration. The HD desorption flux in Figure 7b shows one main peak with a slight shoulder around 1100 K. Only one D_2 desorption peak is present in TDS thermogram shown in Figure 7c. These observations were the same for both alloys and suggest that during the gaseous charging at 873 K, the deuterium is barely trapped by the precipitates and remains almost exclusively in solid solution.

The trapping of hydrogen by the precipitates clearly takes place during the material elaboration process. No contribution associated with a potential deuterium trapping is observed although charging was performed at 873 K, which suggests a very difficult trapping (high energetic barrier for hydrogen in the α-Zr matrix to enter the Nb-containing precipitates). This observation is consistent with some ab-initio calculations performed for steels containing carbides showing very difficult entry of hydrogen into secondary phases [49]. The trapping kinetic constant associated with the interaction of H and the Nb-containing precipitates in M5 was not determined in the present work. Hydrogen detrapping from the precipitates appears to require also a high energy since hydrogen is mainly released when the precipitates dissolve.

The hydrogen species contained in the nuclear fuel claddings mainly comes from the water reduction occurring during corrosion under normal operating conditions and for a very little part from the ternary fission within the uranium oxide fuel. The obtained results indicate that they should not be significantly trapped by the niobium-containing precipitates and should stay in solid solution in the matrix (in the laboratory time scales at least) or precipitate as hydrides. Consequently, the hydrogen trapping by the niobium-containing precipitates has not to be taken into account in the desorption process of the hydrogen absorbed during operation. In the unoxidized state, the desorption kinetics of the hydrogen absorbed by M5 during is identical to the Zy-4 one and is limited by the surface recombination step.

The modelling of the total trapping / detrapping process from the material elaboration to its use in a reactor will be the subject of future studies as well as the interpretations of this trapping /detrapping process during storage or transport of spent fuel.

5 Conclusion

The hydrogen desorption process from unoxidized M5 and Zr-2.5%Nb alloy has been investigated by thermal desorption spectrometry experiments, high sensitivity differential scanning calorimetry and

by using FE modelling programmed with Cast3M code and URANIE optimization tool. The results of these researches are consistent with the following conclusions:

1. Similarly to Zy4, the desorption kinetics of the hydrogen in interstitial solid solution in unoxidized M5 is limited by the surface recombination reaction $2H_{ads} \rightarrow H_2$.
2. The kinetic constant k'_{des} of the surface recombination step is identical to the Zy4 one and is expressed as follows (Eq.10)

$$k'_{des} = 3 \text{ x } 10^{7} \exp\left(-\frac{2.90 \text{ x } 10^{5}\ J\,mol^{-1}}{\text{RT}}\right) \qquad (\text{m}^4\ \text{mol}^{-1}\ \text{s}^{-1}) \qquad \text{(Eq.10)}$$

3. During the elaboration process of M5 and Zr-2.5%Nb, the niobium-containing precipitates trap a part of the hydrogen contained in the alloys. In the studied conditions and regarding M5, the desorption flux corresponding to this initially trapped hydrogen reaches its maximum after the total dissolution of the precipitates, which releases hydrogen into solid solution, indicating a high activation energy for detrapping.
4. During a gaseous deuterium charging of M5 and Zr-2.5%Nb carried out at 873 K up to 100 wtppm, the precipitates did not trap the deuterium, indicating a high activation energy for trapping and suggesting that the hydrogen that is absorbed by the nuclear fuel cladding during normal operating conditions should not be trapped by the precipitates.

6 Acknowledgements

The authors want to thank the Alternative Energies and Atomic Energy Commission (CEA) for funding this research. Framatome and ATI™ are gratefully acknowledged for providing the studied materials.

M5**Framatome** is a trademark or registered trademark of Framatome or its affiliates, in the USA or other countries.

7 References

[1] P. Bossis, D. Pêcheur, K. Hanifi, J. Thomazet, M. Blat, Comparison of the high burn up corrosion on M5 and low tin Zircaloy-4, J. ASTM Int. 3 (2006) 494–525. https://doi.org/10.1520/JAI12404

[2] J.P. Mardon, B. Dunn, Overview of the M5 Alloy behavior under RIA and LOCA Conditions, Proc. 2007 LWR Fuel Perform. Meet. TopFuel 2007 Zero 2010. 40 (2007).

[3] ASTM, Standard Specification for Wrought Zirconium Alloy Seamless Tubes for Nuclear Reactor Fuel Cladding, ASTM B811-13E1, n.d.

[4] S. Suman, M.K. Khan, M. Pathak, R.N. Singh, J.K. Chakravartty, Hydrogen in Zircaloy: Mechanism and its impacts, Int. J. Hydrog. Energy. 40 (2015) 5976–5994. https://doi.org/10.1016/j.ijhydene.2015.03.049.
[5] A. Zieliński, S. Sobieszczyk, Hydrogen-enhanced degradation and oxide effects in zirconium alloys for nuclear applications, Int. J. Hydrog. Energy. 36 (2011) 8619–8629. https://doi.org/10.1016/j.ijhydene.2011.04.002
[6] C. Juillet, M. Tupin, F. Martin, Q. Auzoux, C. Berthinier, F. Miserque, F. Gaudier, Kinetics of hydrogen desorption from Zircaloy-4: Experimental and modelling, Int. J. Hydrog. Energy. 44 (2019) 21264–21278. https://doi.org/10.1016/j.ijhydene.2019.06.034
[7] M.W. Mallet, W.M. Albrecht, Low-Pressure Solubility and Diffusion of Hydrogen in Zirconium, J. Electrochem. Soc. 104 (1957) 142. https://doi.org/10.1149/1.2428522
[8] C. Juillet, M. Tupin, F. Martin, Q. Auzoux, S. Bosonnet, C. Berthinier, Effect of a pre-oxidation on the hydrogen desorption from Zircaloy-4, Corros. Sci. 173 (2020) 108762. https://doi.org/10.1016/j.corsci.2020.108762
[9] www-cast3m.cea.fr/, (n.d.).
[10] F. Gaudier, URANIE: The CEA/DEN Uncertainty and Sensitivity platform, Procedia - Soc. Behav. Sci. 2 (2010) 7660–7661. https://doi.org/10.1016/j.sbspro.2010.05.166
[11] G. Amsel, D. David, G. Beranger, P. Boisot, B. De Gelas, P. Lacombe, Analyse a l'aide d'une methode nucleaire des impuretes introduites dans les metaux par leurs preparations d'etat de surface: Application au zirconium, J. Nucl. Mater. 29 (1969) 144–153. https://doi.org/10.1016/0022-3115(69)90093-2
[12] C.R. Cupp, P. Flubacher, An autoradiographic technique for the study of tritium in metals and its application to diffusion in zirconium at 149° to 240° C, J. Nucl. Mater. 6 (1962) 213–228. https://doi.org/10.1016/0022-3115(62)90272-6
[13] G.U. Greger, H. Münzel, W. Kunz, A. Schwierczinski, Diffusion of tritium in zircaloy-2, J. Nucl. Mater. 88 (1980) 15–22. https://doi.org/10.1016/0022-3115(80)90381-5
[14] A. Sawatzky, The diffusion and solubility of hydrogen in the alpha phase of Zircaloy-2, J. Nucl. Mater. 2 (1960) 62–68. https://doi.org/10.1016/0022-3115(60)90025-8
[15] C. Schwartz, M. Mallet, Observation of the behavior of hydrogen in zirconium, Trans. Am. Soc. Met. 46 (1954) 641–654.
[16] B.F. Kammenzind, D.G. Franklin, H.R. Peters, W.J. Duffin, Hydrogen Pickup and redristribution in alpha annealed Zircaloy-4, Zircon. Nucl. Ind. 11th Int. Symp. ASTM STP 1295. (1996) 338. https://doi.org/10.1520/STP16180S
[17] C.-S. Zhang, B. Li, P.R. Norton, The study of hydrogen segregation on Zr(0001) and Zr(1010) surfaces by static secondary ion mass spectroscopy, work function, Auger electron spectroscopy and nuclear reaction analysis, J. Alloys Compd. 231 (1995) 354–363. https://doi.org/10.1016/0925-8388(95)01847-6
[18] J.H. Austin, T.S. Elleman, K. Verghese, Tritium diffusion in zircaloy-2 in the temperature range −78 to 204° C, J. Nucl. Mater. 51 (1974) 321–329. https://doi.org/10.1016/0022-3115(74)90197-4
[19] D. Khatamian, Diffusion of Hydrogen in Single Crystals of Monoclinic-ZrO2 and Yttrium Stabilized Cubic Zirconia, Defect Diffus. Forum. (2010). https://doi.org/10.4028/www.scientific.net/DDF.297-301.631
[20] S. Sevta, P.S. Ramanjaneyulu, A.S. Kulkarni, M.P. Kumar, M.K. Saxena, R.N. Singh, Studies on diffusion of hydrogen in PWR clad material, J. Radioanal. Nucl. Chem. 324 (2020) 921–927. https://doi.org/10.1007/s10967-020-07126-4
[21] S.C. Lumley, S.T. Murphy, P.A. Burr, R.W. Grimes, P.R. Chard-Tuckey, M.R. Wenman, The stability of alloying additions in Zirconium, J. Nucl. Mater. 437 (2013) 122–129. https://doi.org/10.1016/j.jnucmat.2013.01.335
[22] J.B. Vander Sande, A.L. Bement, An investigation of second phase particles in Zircaloy-4 alloys, J. Nucl. Mater. 52 (1974) 115–118.

[23] X.Y. Meng, D.O. Northwood, Intermetallic precipitates in zircaloy-4, J. Nucl. Mater. 132 (1985) 80–87.
[24] A. Harte, M. Griffiths, M. Preuss, The characterisation of second phases in the Zr-Nb and Zr-Nb-Sn-Fe alloys: A critical review, J. Nucl. Mater. 505 (2018) 227–239. https://doi.org/10.1016/j.jnucmat.2018.03.030
[25] P.A. Burr, S.T. Murphy, S.C. Lumley, M.R. Wenman, R.W. Grimes, Hydrogen accommodation in Zr second phase particles: Implications for H pick-up and hydriding of Zircaloy-2 and Zircaloy-4, Corros. Sci. 69 (2013) 1–4. https://doi.org/10.1016/j.corsci.2012.11.036
[26] P.A. Burr, S.T. Murphy, S.C. Lumley, M.R. Wenman, R.W. Grimes, Hydrogen solubility in zirconium intermetallic second phase particles, J. Nucl. Mater. 443 (2013) 502–506. https://doi.org/10.1016/j.jnucmat.2013.07.060
[27] I.S. Dupim, J.M.L. Moreira, J. Huot, S.F. Santos, Effect of cold rolling on the hydrogen absorption and desorption kinetics of Zircaloy-4, Mater. Chem. Phys. 155 (2015) 241–245.
[28] J. Sayers, S. Ortner, S. Lozano-Perez, Effect of pH on hydrogen pick-up and corrosion in zircaloy-4, Miner. Met. Mater. Ser. Part F9 (2018) 1169–1180. https://doi.org/10.1016/j.matchemphys.2015.02.036
[29] C. Toffolon, J.C. Brachet, T. Guilbert, D. Hamon, S. Urvoy, C. Servant, D. Charquet, L. Legras, J.P. Mardon, Vieillissement thermique des alliages de zirconium-niobium en phase α (570 °C), J. Phys. IV. 11 (2001) 99–108. https://doi.org/10.1051/jp4:2001110
[30] C. Toffolon-Masclet, T. Guilbert, J.C. Brachet, Study of secondary intermetallic phase precipitation/dissolution in Zr alloys by high temperature–high sensitivity calorimetry, J. Nucl. Mater. 372 (2008) 367–378. https://doi.org/10.1016/j.jnucmat.2007.04.042
[31] T. Forgeron, J. Brachet, F. Barcelo, A. Castaing, J. Hivroz, J. Mardon, C. Bernaudat, Experiment and Modeling of Advanced Fuel Rod Cladding Behavior Under LOCA Conditions: Alpha-Beta Phase Transformation Kinetics and EDGAR Methodology, in: G. Sabol, G. Moan (Eds.), Zircon. Nucl. Ind. Twelfth Int. Symp., 2000: pp. 256–278. https://doi.org/10.1520/STP14303S
[32] J.J. Kearns, Terminal solubility and partitioning of hydrogen in the alpha phase of zirconium, Zircaloy-2 and Zircaloy-4, J. Nucl. Mater. 22 (1967) 292–303. https://doi.org/10.1016/0022-3115(67)90047-5
[33] A. McMinn, E.C. Darby, J.S. Schofield, The Terminal Solid Solubility of Hydrogen in Zirconium Alloys, Zircon. Nucl. Ind. Twelfth Int. Symp. (2000) 173–195. https://doi.org/10.1520/STP14300S
[34] E. Zuzek, J.P. Abriata, A. San-Martin, F.D. Manchester, The H-Zr (hydrogen-zirconium) system, Bull. Alloy Phase Diagr. 11 (1990) 385–395. https://doi.org/10.1007/BF02843318
[35] J.J. Kearns, Dissolution kinetics of hydride platelets in Zircaloy-4, J. Nucl. Mater. 27 (1968) 64–72. https://doi.org/10.1016/0022-3115(68)90008-1
[36] IAEA, Waterside corrosion of zirconium alloys in nuclear power plants, Int. At. Energy Agency. TECDOC-996 (1998).
[37] R.L. Tapping, X-ray photoelectron and ultraviolet photoelectron studies of the oxidation and hydriding of zirconium, J. Nucl. Mater. 107 (1982) 151–158. https://doi.org/10.1016/0022-3115(82)90417-2
[38] M. Tupin, F. Martin, C. Bisor, R. Verlet, P. Bossis, J. Chene, F. Jomard, P. Berger, S. Pascal, N. Nuns, Hydrogen diffusion process in the oxides formed on zirconium alloys during corrosion in pressurized water reactor conditions, Corros. Sci. 116 (2017) 1–13. https://doi.org/10.1016/j.corsci.2016.10.027
[39] M. Wilde, K. Fukutani, Penetration mechanisms of surface-adsorbed hydrogen atoms into bulk metals: Experiment and model, Phys. Rev. B. 78 (2008) 115411. https://doi.org/10.1103/PhysRevB.78.115411
[40] A. McNabb, P. Foster, A new analysis of the diffusion of hydrogen in iron and ferritic steels., Trans Met. Soc AIME. 227 (1963) 618–627.
[41] R.A. Oriani, The diffusion and trapping of hydrogen in steel, Acta Metall. 18 (1970) 147–157. https://doi.org/10.1016/0001-6160(70)90078-7

[42] A. Oudriss, J. Creus, J. Bouhattate, E. Conforto, C. Berziou, C. Savall, X. Feaugas, Grain size and grain-boundary effects on diffusion and trapping of hydrogen in pure nickel, Acta Mater. 60 (2012) 6814–6828. https://doi.org/10.1016/j.actamat.2012.09.004
[43] C. Hurley, F. Martin, L. Marchetti, J. Chêne, C. Blanc, E. Andrieu, Numerical modeling of thermal desorption mass spectroscopy (TDS) for the study of hydrogen diffusion and trapping interactions in metals, Int. J. Hydrog. Energy. 40 (2015) 3402–3414. https://doi.org/10.1016/j.ijhydene.2015.01.001
[44] H.E. Kissinger, Reaction kinetics in differential thermal analysis, Anal. Chem. 29 (1957) 1702–1706. https://doi.org/10.1021/ac60131a045
[45] W.Y. Choo, J.Y. Lee, Thermal analysis of trapped hydrogen in pure iron, Metall. Trans. A. 13 (1982) 135–140. https://doi.org/10.1007/BF02642424
[46] F.G. Wei, T. Hara, K. Tsuzaki, Precise determination of the activation energy for desorption of hydrogen in two Ti-added steels by a single thermal-desorption spectrum, Metall. Mater. Trans. B. 35 (2004) 587–597. https://doi.org/10.1007/s11663-004-0057-x
[47] K. Ebihara, H. Kaburaki, Numerical modeling of thermal desorption spectra of hydrogen: a review of thermal desorption models, ISIJ Int. 52 (2012) 181–186. https://doi.org/10.2355/isijinternational.52.181
[48] C. Toffolon, Etude métallurgique et calculs des diagrammes de phases des alliages base zirconium du système : Zr-Nb-Fe-(O,Sn), Université Paris 6, 2000.
[49] D. Di Stefano, R. Nazarov, T. Hickel, J. Neugebauer, M. Mrovec, C. Elsässer, First-principles investigation of hydrogen interaction with TiC precipitates in alpha-Fe, Phys. Rev. B. 93 (2016) 184108. https://doi.org/10.1103/PhysRevB.93.184108

Comparison between transformed fraction of βNb → βZr obtained by calorimetry (dashed lines, the left ordinates) and hydrogen desorption flux (continuous lines, right ordinates) on as-received M5 samples submitted to a 10 K min^{-1} (black lines) and 3 K min^{-1} (blue lines) temperature ramp as function of temperature. Gaussian peak deconvolutions into 2 peaks of the TDS data are shown in dotted lines.